

# Droplet-Based Microfluidics Platform for the Synthesis of Single-Atom Heterogeneous Catalysts

Thomas Moragues, Sharon Mitchell,\* Dario Faust Akl, Javier Pérez-Ramírez,\* and Andrew deMello\*

Wet chemical approaches are among the most versatile and scalable strategies for preparing single-atom heterogeneous catalysts (SACs). However, despite their broad application, the synthesis of SACs via these routes remains largely ad hoc, with limited attention to the effect of different synthetic parameters on the stabilization of metal species. As a proof of concept, herein, a microfluidic platform is demonstrated for short-timescale ( $<10$  s), systematic syntheses of SACs via wet impregnation using a range of metal precursor–carrier combinations. The microfluidic environment within rapidly mixed, nanoliter droplets ensures precise control of the concentrations and residence times of the support particles in the metal precursor solutions. This enables the rapid assessment of the influence of the metal precursor concentration on the uptake and dispersion of the adsorbed metal species, as demonstrated for the synthesis of palladium and platinum SACs based on a high-surface form of graphitic carbon nitride ( $C_3N_4$ ). Extension to SACs based on other metals (Ni) and relevant carriers (N-doped carbon,  $\gamma$ -alumina) confirms the generality of the synthesis method. The microfluidic approach opens possibilities for high-throughput parameter screening and mechanistic studies in the design of heterogeneous single-atom catalysts.

wet-chemical, solid-state, and gas-phase routes.<sup>[3]</sup> Among these, the postsynthetic wet impregnation of metal precursors is of great interest as a cheap, versatile, and scalable route.<sup>[4]</sup> The main challenge in fabricating SACs is the propensity of metal atoms to aggregate into clusters or nanoparticles during synthesis, especially with increasing metal contents, which are desirable to maximize reactor productivity.<sup>[5]</sup> In this context, it is known that the provision of carriers with coordination sites able to react and anchor with metal precursors, such as functionalized carbons, carbon nitrides, and certain metal oxides, is critical.<sup>[6–8]</sup> Still, the synthesis is typically approached in an ad hoc manner with limited knowledge of the adsorption processes or the impact of the conditions on the uptake and dispersion of metal species. Hence, a more systematic exploration of the parameter space on the carriers as well as deeper understanding of the adsorption properties of metal ions is needed to 1) allow for controlled, reproducible


## 1. Introduction

High-performance catalysts are critical in fulfilling the sustainability goals of the 21st century. Recently, single-atom heterogeneous catalysts (SACs), formed by spatially isolated metal centers stabilized at the surface of suitable carrier materials, have received much attention because of the high metal utilization, atomic definition, and unique reactivity they potentially offer.<sup>[1,2]</sup> Many synthesis methods have been reported, including

SACs synthesis, 2) assess the potential of novel SAC carrier materials, and 3) enable the efficient synthesis of high-density SACs.

Over the last two decades, droplet-based microfluidics has evolved at an astonishing rate, developing and refining diverse droplet-based structures, components, workflows, and concepts.<sup>[9,10]</sup> Droplet-based systems maintain the intrinsic advantages of traditional microfluidic platforms (including small instrumental footprints, the ability to process reduced sample volumes, the facile integration of functional components, and the exquisite control of mass and heat transport) while providing for dramatic improvements in analytical throughput, preventing surface molecule interactions, and enhancing fluidic mixing.<sup>[11]</sup> The advantages of droplet-based microfluidic reactors over flask-based methods for materials synthesis are now well recognized, and they have been exploited to synthesize materials with finely tailored properties.<sup>[12–14]</sup> Nevertheless, perhaps the most compelling capability of these platforms relates to the ease with which thousands of discrete reactions may be performed in an ultrahigh throughput fashion,<sup>[15]</sup> allowing for efficient screening of parameter space or reaction discovery.<sup>[16]</sup> That said, despite their extensive use in the field of biochemistry, e.g., for droplet digital polymerase chain reaction (ddPCR),<sup>[17]</sup> their applications in chemical synthesis are more recent. In the catalysis field, the

T. Moragues, S. Mitchell, D. Faust Akl, J. Pérez-Ramírez, A. deMello  
Institute of Chemical and Bioengineering  
ETH Zürich  
Vladimir-Prelog-Weg 1-5/10, 8093 Zürich, Switzerland  
E-mail: msharon@chem.ethz.ch; jpr@chem.ethz.ch;  
andrew.demello@chem.ethz.ch

 The ORCID identification number(s) for the author(s) of this article can be found under <https://doi.org/10.1002/ssstr.202200284>.

© 2022 The Authors. Small Structures published by Wiley-VCH GmbH. This is an open access article under the terms of the Creative Commons Attribution License, which permits use, distribution and reproduction in any medium, provided the original work is properly cited.

DOI: 10.1002/ssstr.202200284

use of continuous flow microfluidics has notably enabled the synthesis of polymer-stabilized nanometer size metal clusters of superior catalytic activity compared to their batch-prepared counterparts,<sup>[18]</sup> while droplet-based microfluidic platforms have been widely employed to synthesize metal nanoparticles of precisely tuned size distribution, and thus catalytic performance.<sup>[19–21]</sup> Yet, to the best of our knowledge, the deposition of metal species on solid supports has not been studied, although it has the potential to provide valuable insights into the preparation of SACs via wet impregnation. Accordingly, herein we describe a method in which droplet-based microfluidic reactors are used to rapidly and reproducibly prepare highly dispersed single atoms of user-defined species on chemically-distinct supports for the first time (**Figure 1**). As a proof of concept, the high level of control of our method is demonstrated for the synthesis of Pd and Pt-supported carbon nitride single-atom catalysts, performed within 10 s. The variation in metal uptake with pH indicates a strong dependence on electrostatic interactions. Overall, our approach, which we generalize to various relevant metal/carrier systems, serves as a baseline for the high-throughput screening of parameter space in SAC synthesis.

## 2. Results and Discussion

The developed synthesis platform leverages droplet-based microfluidics to produce highly reproducible, single reactor vessels, containing equal amounts of aqueous metal precursor solution and carrier material suspension. The device includes a cross-flow junction for droplet generation, followed by an incubation channel (total length 1 m), coiled on a surface of 100 mm<sup>2</sup> (**Figure 1b**). This structure allows for fast and efficient mixing, through chaotic advection (**Figure 1c**),<sup>[22]</sup> achieved within 250 ms after the first contact between the carrier and metal precursor streams. The timescale is at least two orders of magnitude faster than for commonly used batch preparations, where mixing times depend on the mixing apparatus, the volume of the reactor, the temperature, and the concentrations involved. The continuous oil phase plays two roles, 1) shearing the aqueous streams to form the droplets and 2) wetting the channel walls to prevent surface-synthesis media interactions.

The dosing of solid suspensions is particularly challenging in continuous flow systems as channel blockage jeopardizes process operation. At larger scales, subsequent pressure buildups can lead to safety hazards, including reactor rupture and

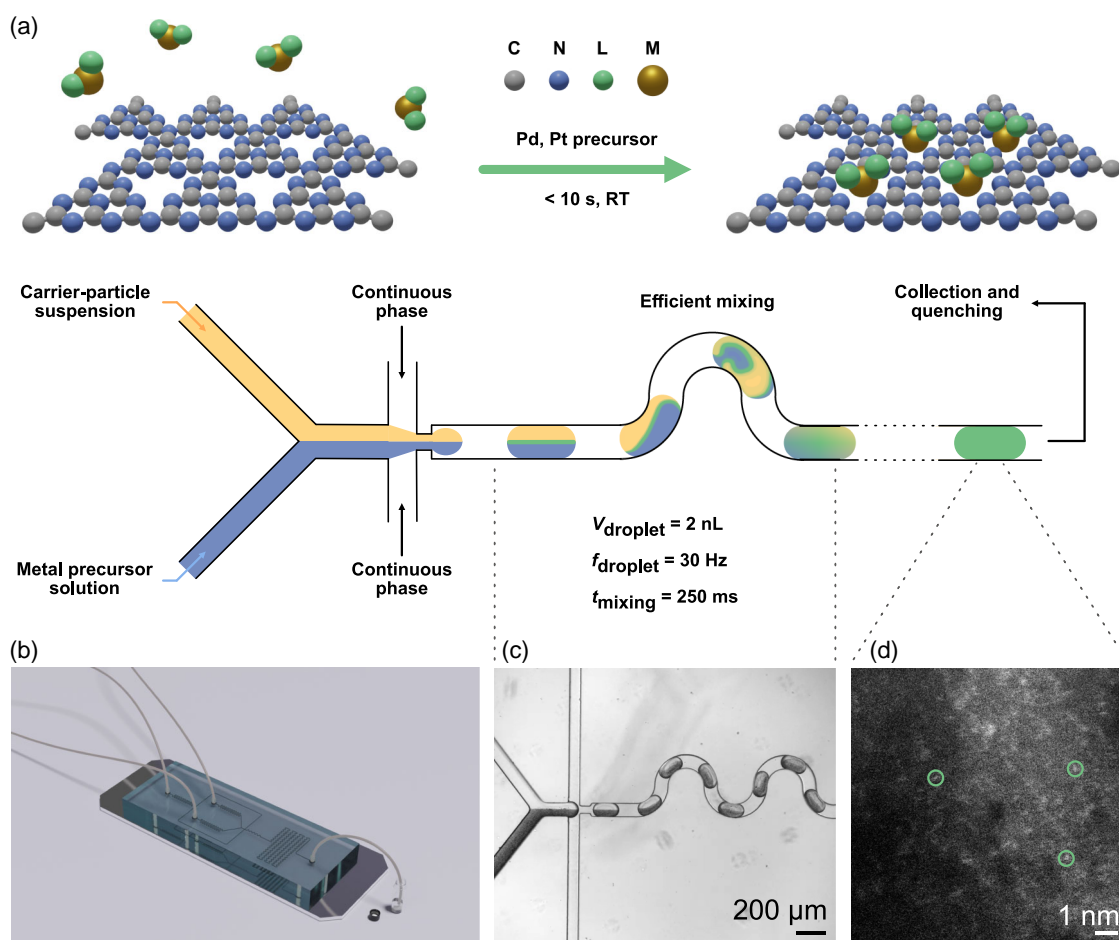


**Figure 1.** a) Droplet-based microfluidic synthesis of SACs by wet impregnation. b) 3D rendering of the microfluidic device used in this work. c) Bright-field image of water-in-oil droplets containing the metal precursor (ML<sub>x</sub>) and carrier with efficient mixing. d) Aberration-corrected annular dark field scanning transmission electron microscopy (AC-ADF-STEM) image confirming the presence of isolated metal atoms in the materials obtained by microfluidic synthesis.

explosion. The use of droplet-based microfluidics to compartmentalize the solid partially addresses this issue. However, channel clogging and fouling can still occur before the cross-junction (Figure S1, Supporting Information), as well as settling in the syringe. Therefore, particle size distributions were optimized (Figure S2, Supporting Information) using ultrasonication. Notably, larger particles will cause clogging by acting as favored aggregation centers for smaller particles. If aggregation occurs in the syringe, settling will necessarily follow and dosing will not be uniform with time. Experimentally, the optimal particle size distribution was found to be between 0.2 and 10  $\mu\text{m}$ . The concentration of the carrier suspension ( $5 \text{ g L}^{-1}$ ) used in this study to avoid reactor clogging. Comparable uptakes were evidenced with decreasing concentrations of the carrier suspension ( $2.5 \text{ g L}^{-1}$ ) at constant metal: carrier wt% ratio (sample  $\text{C}_3\text{N}_4\text{-PdNH}_3\text{-100-3}$ , Table S1, Supporting Information). The platform is highly robust to different metal precursor solutions, the main restriction being the solubility of the metal salt in a given solvent. Here, we studied adsorption processes from aqueous solutions due to their practical relevance, but it is possible to operate with other solvents reported for SAC synthesis (e.g., methanol, ethanol, acetonitrile, or acetone).

Isolation of the supported metal catalysts requires the collection of droplets and quenching of the synthesis by dilution. The procedure leads to a total transient time of 131 s between the first contact of the two streams and quenching. The additional residence time outside the microfluidic device ( $\tau_{\text{tubing}}$ ) does not impact impregnation because no mixing occurs, resulting in purely diffusive ion migration (Note S1, Supporting Information). While previously reported batch syntheses have been performed over several hours or days,<sup>[23,24]</sup> we demonstrate in our platform the synthesis of  $\text{Pd/C}_3\text{N}_4$  and  $\text{Pt/C}_3\text{N}_4$  SACs within 10 s of internal chip residence time ( $\tau_{\text{chip}}$ ).

The performance of the microfluidic platform was evaluated for the synthesis of Pd- and Pt-SACs based on a high-surface form of graphitic carbon nitride ( $\text{C}_3\text{N}_4$ ) using distinct metal precursors commonly applied for SAC synthesis (Table S2,

Figure S3, Supporting Information). Comparison of the metal uptakes in resulting materials as a function of the metal:carrier wt% ratio during the synthesis provides insights into the relative adsorption behavior. In the microfluidic syntheses of  $\text{Pd/C}_3\text{N}_4$  systems (Figure 2a), almost all the metal precursor present in solution (nominal) adsorbs onto the carrier. As the metal concentration increases and the surface progressively saturates, the uptake eventually deviates from the amount initially present in the solution. Both palladium precursors studied exhibited similar trends. Comparatively, in the synthesis of  $\text{Pt/C}_3\text{N}_4$ , substantially lower metal uptakes resulted (2 to 3 times).

The differences in the amounts of Pd and Pt deposited on the  $\text{C}_3\text{N}_4$  support can be rationalized based on the synthesis conditions, which impact the electrostatic interactions of metal complexes on carrier surfaces.<sup>[25,26]</sup> In particular, the structure of  $\text{C}_3\text{N}_4$  contains functional groups, including various amines, that can react with protons or hydroxyl groups and acquire positive or negative surface charges, respectively. We determined the isoelectric point (IEP) of particle suspensions of  $\text{C}_3\text{N}_4$  to be 4.5 (Figure 3a), consistent with previous literature reports.<sup>[27]</sup> Calculation of the pH values in the droplets (Figure 3b) revealed that the conditions favor adsorption for every precursor except for  $\text{K}_2[\text{Pt}(\text{CN})_4]$  (pH 7.3–8.3), which would require a lower pH for optimal adsorption, explaining the limited uptake measured for this precursor. Comparatively, for  $\text{H}_2\text{PtCl}_6$ , the pH values (3–4 depending on the concentration) are close to the IEP (4.5), indicating that the adsorption will likely be suboptimal. To further confirm the electrostatic nature of the adsorption mechanism, we repeated the synthesis with  $\text{H}_2\text{PtCl}_6$ , decreasing the pH to match the conditions employed for  $\text{PdCl}_2$  (1–2). As expected, the reduced pH inside the droplets led to an increased Pt uptake to similar levels observed for the Pd-based catalysts.

The nuclearity of the deposited metal species in the microfluidically prepared materials was assessed by HAADF-STEM. When using  $[\text{Pd}(\text{NH}_3)_4](\text{NO}_3)_2$  as a precursor, clusters and small nanoparticles were evidenced when using  $\text{Pd/C}_3\text{N}_4$  ratios higher than 1:100 (i.e., 1:50 and 1:20). Thus, this ratio was identified as

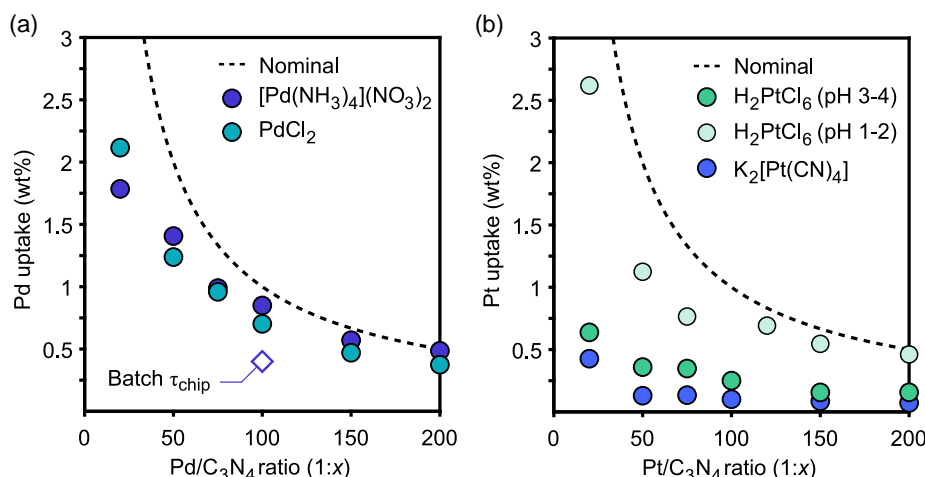


**Figure 2.** a) Pd and b) Pt uptakes determined in samples prepared by microfluidic synthesis with varying M/ $\text{C}_3\text{N}_4$  ratio (M = Pd or Pt), using  $[\text{Pd}(\text{NH}_3)_4](\text{NO}_3)_2$ ,  $\text{PdCl}_2$ ,  $\text{H}_2\text{PtCl}_6$ , or  $\text{K}_2[\text{Pt}(\text{CN})_4]$  as precursors, with an internal chip residence time ( $\tau_{\text{chip}}$ ) of 9 s and a total transient time ( $\tau_{\text{total}}$ ) of 131 s. In (a), Pd uptake obtained in a standard batch synthesis using  $[\text{Pd}(\text{NH}_3)_4](\text{NO}_3)_2$  and a 1:100 M/ $\text{C}_3\text{N}_4$  ratio for an impregnation time equivalent to  $\tau_{\text{chip}}$  (9 s), and in (b), the synthesis using  $\text{H}_2\text{PtCl}_6$  with reduced pH, are shown for comparison. Error bars are smaller than the symbol size.

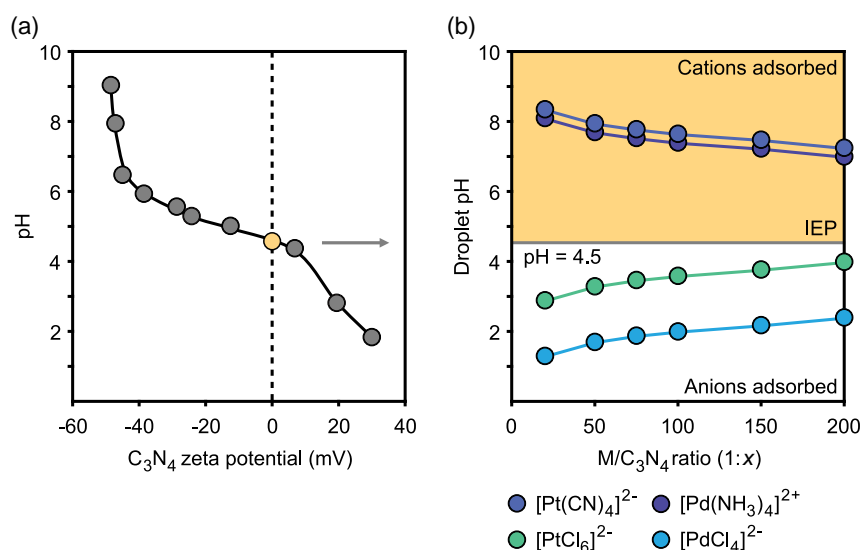


**Figure 3.** a) Calculated pH values inside the droplets for all precursors concentrations used in Figure 2a, b. Evolution of the zeta potential in suspensions of  $C_3N_4$  of various pH. The isoelectric point (IEP) is interpolated from the zero-zeta potential. Error bars are smaller than the symbol size.

the threshold under which atomically dispersed Pd metal centers could be stabilized in the absence of nanoparticles under these conditions (Figure 4). In contrast, when using  $PdCl_2$ , clusters of metal salts were observed (Figure S4, Supporting Information) at every ratio tested, likely indicating a different stabilization interaction. At ratios below 1:100, no nanoparticles were observed with  $K_2[Pt(CN)_4]$  (Figure S5, Supporting Information), while atomic dispersions only resulted in the case of a metal:carrier ratio of 1:200 for  $H_2PtCl_6$  (Figure S6, Supporting Information). Interestingly, when decreasing the

pH for  $H_2PtCl_6$ , no nanoparticles were observed at ratios below 1:100, likely a consequence of the increased binding sites availability induced by favorable pH conditions (Figure S7, Supporting Information). Finally, to further showcase the operational flexibility of the platform, syntheses using different metal centers and carriers were performed. First,  $Ni(NO_3)_2$  was impregnated on N-doped carbon (N-C) and yielded atomically dispersed  $Ni(II)$  with initial conditions of 1:75 ratio (Figure S8a, Supporting Information), which can be rationalized from the considerably higher surface area of the carrier.

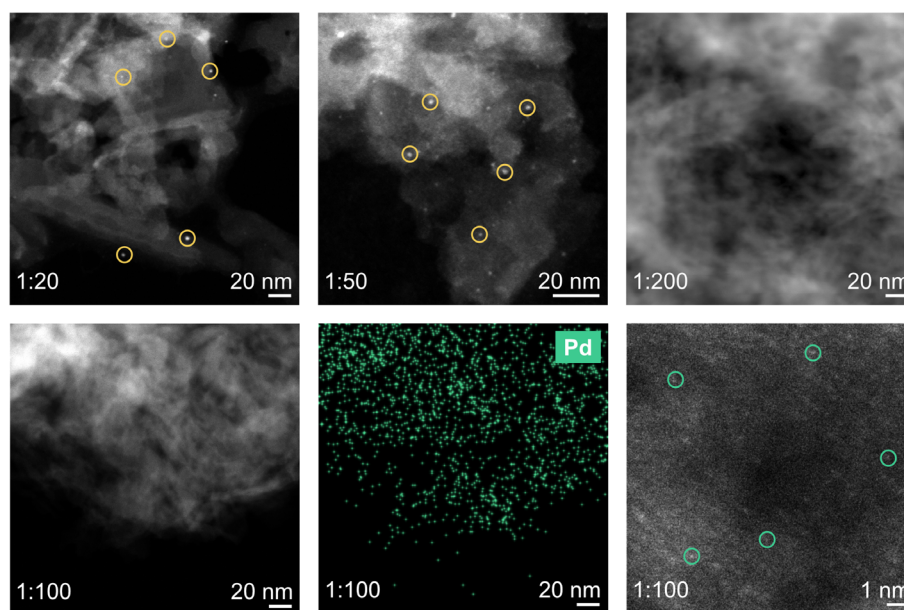


**Figure 4.** High-angle annular dark field scanning transmission electron microscopy (HAADF-STEM) micrographs of the microfluidically prepared materials obtained in the synthesis of  $Pd/C_3N_4$  using  $[Pd(NH_3)_4](NO_3)_2$  at various  $Pd/C_3N_4$  ratios. An energy-dispersive X-ray spectroscopy map and an aberration-corrected annular dark field STEM image confirm the uniform distribution and atomic dispersion of Pd in the sample prepared with a 1:100 ratio. Nanoparticles and single Pd atoms are circled in yellow and green, respectively.

Additionally,  $[\text{Pd}(\text{NH}_3)_4](\text{NO}_3)_2$  was atomically dispersed on a commercially available  $\gamma\text{-Al}_2\text{O}_3$  using a very low initial ratio (1:526) (Figure S8b, Supporting Information). The formation of nanoparticles at higher nominal metal concentrations could be explained by the low surface area of this carrier and the fact that  $\gamma\text{-Al}_2\text{O}_3$  typically requires activating treatments to generate sufficient coordination sites to stabilize higher metal contents. The comparatively low uptake observed is consistent with the unfavorable pH (7–8) in the synthesis compared to the IEP of  $\gamma\text{-Al}_2\text{O}_3$ , of about 8.<sup>[25]</sup> These results demonstrate the potential of using microfluidic platforms for the short-timescale, systematic preparation of SACs with diverse metal–carrier combinations under a variety of synthesis conditions.

For comparative purposes,  $\text{Pd}/\text{C}_3\text{N}_4$  and  $\text{Pt}/\text{C}_3\text{N}_4$  SACs were prepared by standard batch methods (Figure 5). The lower uptakes compared to the microfluidic syntheses with equivalent residence times highlight the efficient and rapid mixing inherent to the small scale of the microfluidic platform. When run for longer times, the  $\text{Pd}/\text{C}_3\text{N}_4$  batch syntheses eventually yielded similar uptakes to those performed within the microfluidic platform (Figure 2a), confirming the transferability of the results between the two synthetic approaches. As for  $\text{Pt}/\text{C}_3\text{N}_4$ , the higher uptakes obtained in batch compared to microfluidic syntheses prove that unfavorable conditions (pH 3–4) act as kinetic limitations that can be overcome by extending the reaction time. Thus, depending on the desired carrier and metal precursor, the experimenter must carefully choose the pH when working with the microfluidic platform to ensure that such limitations are avoided.

Droplet-based microfluidics is not yet a scalable approach for single-atom catalyst synthesis. However, it is a powerful tool for discovery because of its ability to exert control over mixing and synthesis conditions as well as its high-throughput nature. To fully take advantage its potential, the integration of analytical techniques suitable for pL–nL scale detection is key. Currently, sample properties are extracted through the isolation of the catalyst off-device and subsequent characterization by

inductively coupled plasma optical emission spectrometry (ICP-OES) and STEM. With a view to performing the screening of synthesis parameter spaces, integrating an in-line detection technique allowing the quantification of the metal uptake would be highly advantageous. The challenge here resides in the technique sensitivity, analytical throughput, and selectivity, which should differentiate between adsorbed and free metal ions. Although recent studies have showcased in-droplet broadband absorption spectroscopy,<sup>[28]</sup> the presence of scattering solids in our droplets would likely induce appreciable noise. X-ray absorption spectroscopy (XAS),<sup>[29]</sup> while highly specialized, could also provide insights into the coordination environment of the metal centers as well as means to go beyond nuclearity assessment, studying the speciation of metals as they adsorb to carrier surfaces. A platform is currently being developed that will enable the operando, in-droplets study of precursor adsorption by XAS. Quenching impregnation in-line to remove unadsorbed metal ions could also be envisaged with a classical droplet splitting approach<sup>[30]</sup> combined with acoustophoresis<sup>[31,32]</sup> or centrifugal separation, both of which would become easier with the progressive aggregation of the carrier particles observed along the flow path (Figure S9, Supporting Information). Subsequently, in-droplet fluorescence spectroscopy<sup>[33]</sup> of picoinjected molecular probes<sup>[34]</sup> enabled or quenched by metal ions could be used to directly or indirectly quantify the metal uptake on the carriers. Another interesting prospect is the direct use of microfluidically prepared catalysts for chemical reactions inside the droplet itself. Here, detection of a relevant product could provide a selection parameter for catalyst collection and in-depth analysis with classical out-of-device workflows.

Finally, the short timescales and levels of control showcased by our method suggest the potential to derive adsorption kinetics of metal precursors on carriers, for example, by quantifying metal uptakes as a function of residence time using low metal precursor concentrations. Here, when increasing the residence time, e.g., by decreasing the flow rates, particular attention should be paid to the impact of droplet speed and volume with the view of keeping the mixing efficiency constant that will likely require further design optimization. Additionally, and although industrially relevant SACs syntheses are performed at room temperature, the rapid heat transfer at the small scale could be leveraged by implementing a heating stage to study impregnation at various temperatures, similar to already-developed platforms for enzymes<sup>[35]</sup> or nanocrystal synthesis kinetics.<sup>[36]</sup>

### 3. Conclusions

In summary, we have demonstrated a droplet-based microfluidic platform for the synthesis of SACs, taking advantage of the superior mixing and mass transfer control offered by the approach. Under appropriate conditions, we obtained single Pd and Pt atomic centers stabilized on graphitic carbon nitride within just 10 s, confirming the electrostatic nature of the adsorption mechanism and highlighting the rapid kinetics. The metal content of the carriers, determined by ICP-OES, was correlated with the observed metal dispersion, assessed with STEM, permitting the identification of thresholds under which atomically-dispersed species are stabilized. Differences in observed metal uptakes,

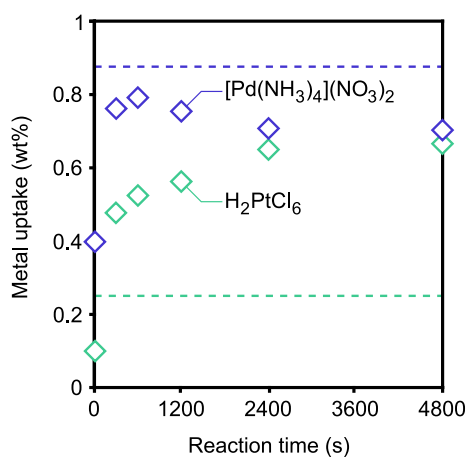


**Figure 5.** Pd and Pt uptake obtained in batch syntheses using  $[\text{Pd}(\text{NH}_3)_4](\text{NO}_3)_2$  and  $\text{H}_2\text{PtCl}_6$  at a 1:100 M/ $\text{C}_3\text{N}_4$  ratio for increasing impregnation times. Dotted lines show uptakes obtained for the same ratio within the microfluidic platform. Error bars are smaller than the symbol size.



evidenced when using distinct metal precursors, could be rationalized based on the synthesis conditions. The applicability to diverse metal precursors and support materials highlighted the versatility of the microfluidic platform. We firmly believe this work constitutes an important step toward high-throughput screening of parameter spaces that would undoubtedly enhance discovery and understanding in the design of single-atom catalysts.

## 4. Experimental Section

**Fabrication of the Microfluidic Device:** The microfluidic device is a single-layer elastomeric device fabricated following standard soft lithography procedures.<sup>[37]</sup> The design was drawn on AutoCAD and printed as a high-resolution photolithographic mask (Micro Lithography Services Ltd., Chelmsford, UK). Using a SU-8 photoresist (Gersteltec, Pully, Switzerland), a 90  $\mu\text{m}$ -thick master mold was created on a 100 mm diameter silicon wafer through standard photolithography. The obtained mold was exposed to a chlorotrimethylsilane (Sigma-Aldrich, Buchs, Switzerland) atmosphere for 2 h in a desiccator at a pressure of 80 mbar. Subsequently, a polydimethylsiloxane (PDMS)-curing agent mixture (10:1 weight basis, Elastosil RT 601 components A and B, Wacker Chemie AG, Munich, Germany) was poured onto the mold, degassed in a desiccator for 45 min, and cured for 1 h at 343 K. The PDMS was then peeled from the mold and cut into the desired shape. Inlets and outlets of 0.76  $\mu\text{m}$  diameter were pierced through using a hole puncher (Syneo, Florida, USA). Finally, the PDMS was bonded to a regular microscope glass slide after surface activation in an air-plasma oven (EMITECH K1000X, Quorum Technologies, East Sussex, UK).

**Operation of the Microfluidic Device:** To control the flow rate in the device, precision neMESYS syringe pumps (CETONI GmbH, Korbussen, Germany) were used in conjunction with gastight 5 and 1 mL syringes (Hamilton AG, Bonaduz, Switzerland) for the continuous phase (A) and the aqueous phases (B, C), respectively. Typically, for a total flow rate of 10  $\mu\text{L min}^{-1}$ , the flow rate was set to 5.55  $\mu\text{L min}^{-1}$  for the continuous phase and 2.22  $\mu\text{L min}^{-1}$  for each aqueous phase inlet. To connect the syringes to the device, PTFE tubing (1/16 in. OD  $\times$  0.010 in. ID, Thermo Fisher Scientific, Waltham, USA) and Tygon tubing (Tygon S-54-HL, i.d. 250  $\mu\text{m}$ , Thermo Fisher Scientific, Waltham, USA) were used, linked together with metal pins (TE Needle 30 GA  $\frac{1}{2}$  in. Lavender, Buchsteiner GmbH, Gingen, Germany). The obtained 2 nL water-in-oil droplets were generated at a frequency of 30 Hz. The operation of the system was monitored using a MotionPro Y series high-speed camera (IDTVision, Pasadena, USA) mounted on an Eclipse Ti-E inverted microscope (Nikon) equipped with a motorized stage (Mad City Labs, Madison, USA).

**Carrier Preparation:** Calcination of dicyandiamide (10 g, Sigma-Aldrich, Buchs, Switzerland) at 823 K (2.3 K  $\text{min}^{-1}$ ) for 4 h in static air yielded graphitic carbon nitride in bulk form (BCN).<sup>[38]</sup> Then, BCN (2 g) was exfoliated by thermal treatment at 773 K for 10 h (2.3 K  $\text{min}^{-1}$ ) in static air, leading to exfoliated carbon nitride ( $\text{C}_3\text{N}_4$ ). N-doped carbon was prepared by doping mesoporous carbon with nitrogen using dicyanamide according to a previously reported procedure.<sup>[39]</sup>  $\gamma$ -alumina was acquired commercially (nanopowder for TEM, <50 nm, Sigma-Aldrich, Buchs, Switzerland).

**Microfluidic Metal Introduction and Work-Up:** The pristine carrier powders (25 mg) were dispersed in Mili-Q purified water (5 mL) and sonicated with a strong ultrasound probe (Sonopuls UW 2070, 60% max power, Bandelin GmbH, Berlin, Germany) for 5 min to yield a 5 g  $\text{L}^{-1}$  suspension of appropriate particle size distribution (see Figure S2, Supporting Information). In the meantime, a 0.05 g  $\text{L}^{-1}$  aqueous metal precursor solution was also prepared in Mili-Q purified water (5 mL). In the microfluidic device, syringes A, B, and C were loaded with fluorinated oil (A) (HFE-7500, 3M), the carrier suspension (B), and the metal precursor solution (C). With the aforementioned concentrations, generated droplets containing the carrier and the metal precursor (1:20 to 1:200 wt% ratio) were collected for 45 min at the outlet in a stirred vial containing Mili-Q purified

water (3.8 mL) to quench the impregnation by dilution and 1H,1H,2H,2H-perfluoro-1-octanol (100  $\mu\text{L}$ , Apollo Chemicals Ltd., Tamworth, UK) was added to break the emulsion. The solid was allowed to settle, and then most of the liquid was removed using a disposable syringe. Next, the solid was dried in a 338 K oven overnight, before being weighed and parted into two samples for imaging in HAADF-STEM and palladium quantification using ICP-OES, respectively. Good repeatability over a series of five collection experiments verified the precision of our solid dosing (Table S3, S4, Supporting Information) as well as of the metal uptake quantification by ICP-OES (Table S5, Supporting Information).

Following this procedure, supported Pd on  $\text{C}_3\text{N}_4$  was prepared from tetraamminepalladium(II) nitrate solution (abcr GmbH, Karlsruhe, Germany) in Mili-Q water, or palladium chloride (abcr GmbH, Karlsruhe, Germany) dissolved in hydrochloric acid (100 mM), alternatively. Supported Pt on  $\text{C}_3\text{N}_4$  was prepared from potassium tetracyanoplatinate(II) hydrate (Sigma-Aldrich, Buchs, Switzerland) or chloroplatinic acid hexahydrate (abcr GmbH, Karlsruhe, Germany), dissolved in Mili-Q water or in hydrochloric acid (100 mM), depending on the required pH. Supported Ni on N-doped carbon (N-C) was prepared from Ni(II) nitrate (Strem Chemicals Inc., Newburyport, USA). Supported Pd on  $\gamma$ -alumina was prepared from the same 5 wt% tetraamminepalladium(II) nitrate solution. For each, keeping the residence time constant, the metal:carrier ratio was varied by adjusting the precursor concentration in the droplets.

**Batch Metal Introduction:** For the batch process, the same  $\text{C}_3\text{N}_4$  suspension (500  $\mu\text{L}$ ) and Pd(II) precursor solution (500  $\mu\text{L}$ ) were added to a vial and stirred for 9 s (or 131 s alternatively). Then, Mili-Q purified water (19.5 mL), HFE-7500 (1.25 mL), and 1H,1H,2H,2H-perfluoro-1-octanol (500  $\mu\text{L}$ ) were added to quench the impregnation and reproduce the experimental conditions of the microfluidic experiment. From there, the work-up and characterization were the same as previously described.

**Characterization:** The size distribution of the  $\text{C}_3\text{N}_4$  suspension in water was obtained using a Malvern Panalytical Mastersizer 3000 (Malvern Instruments, Malvern, UK) laser diffraction instrument. An ultrasonication probe (40 W max, 40 kHz) is used in the device to prevent agglomeration of the particles (mild ultrasonication). The specific surface area of the carriers was estimated from the Brunauer–Emmett–Teller (BET) theory on a Tristar II 3020 instrument (Micromeritics, Norcross, USA) measuring the  $\text{N}_2$  (for  $\text{C}_3\text{N}_4$  and  $\text{Al}_2\text{O}_3$ ) or Ar (for N-C) adsorption on the carriers, which were previously degassed overnight at 423 K under vacuum. The adsorption average pore diameter was determined with the 4 V  $\text{A}^{-1}$  equation (BET) for  $\text{C}_3\text{N}_4$  and  $\text{Al}_2\text{O}_3$  while the median pore width was obtained from the Horváth–Kawazoe method for N-C. The metal content was measured with a Horiba Ultima 2 (Kyoto, Japan) ICP-OES. Prior to analysis, the solids were digested overnight in mixtures of hydrogen peroxide (1 mL, 30 wt%, Thermo Fisher Scientific, Waltham, USA) and either sulfuric acid (3 mL, conc., Sigma-Aldrich, Buchs, Switzerland), or nitric acid (3 mL, >65 wt%, Sigma-Aldrich, Buchs, Switzerland). The Pt samples were additionally treated with aqua regia (0.5 mL) for 3 h. The pH of the precursor solutions was measured using a JENWAY 3505 pH meter (Cole-Parmer Ltd., Vernon Hills, USA) calibrated with pH 4 and pH 7 standard solutions before use. Zeta potential measurements of the  $\text{C}_3\text{N}_4$  suspensions (0.05 wt% in Mili-Q water) were carried out in a Malvern Panalytical Zetasizer Nano series instrument (Malvern, UK). The isoelectric point (IEP) is interpolated at zeta potential equals zero when varying the pH of the suspension. Metal-supported samples were analyzed in a Talos F200X microscope (200 kV, Thermo Fisher Scientific, Waltham, USA) equipped with and energy-dispersive X-ray spectroscopy detector under conventional HAADF-STEM or with a Hitachi HD2700CS microscope (200 kV, Tokyo, Japan) in aberration-corrected (AC-ADF-STEM) mode. The purpose of this last setup is to achieve pure atomic number (Z) contrast thanks to a probe corrector (CEOS) to avoid any Bragg diffraction. The samples were dispersed in ethanol and drop-casted onto copper TEM grids coated with a lacey carbon foil, followed by subsequent drying in a 338 K oven. The pH of the suspensions was adjusted to the desired values using HCl (1 mM) and NaOH (1 mM). X-ray diffraction (XRD) of

the pristine carrier powders was carried out in an X'Pert PRO MPD diffractometer (Malvern Instruments, Malvern, UK) using Bragg–Brentano geometry and Ni-filtered Cu K $\alpha$  ( $\lambda = 0.1541$  nm) radiation. Diffraction patterns were acquired from 5° to 70° 2 $\theta$  (0.05° step size; 1.5 s per step).

## Supporting Information

Supporting Information is available from the Wiley Online Library or from the author.

## Acknowledgements

This work was created as a part of NCCR Catalysis (grant no. 180544), a National Centre of Competence in Research funded by the Swiss National Science Foundation. The authors thank the Scientific Center for Optical and Electron Microscopy at the ETH Zürich, ScopeM for access to their facilities, and Dr. Alla Sologubenko for training.

## Conflict of Interest

The authors declare no conflict of interest.

## Data Availability Statement

The data that support the findings of this study are openly available in [Zenodo] at [https://doi.org/10.5281/zenodo.7107186], reference number [7107186].

## Keywords

droplet microfluidics, metal dispersion, single-atom heterogeneous catalysts, synthesis methods, wet impregnation

Received: September 26, 2022

Revised: November 14, 2022

Published online: December 29, 2022

- [1] S. K. Kaiser, Z. Chen, D. Faust Akl, S. Mitchell, J. Pérez-Ramírez, *Chem. Rev.* **2020**, 120, 11703.
- [2] R. Qin, P. Liu, G. Fu, N. Zheng, *Small Methods* **2018**, 2, 1700286.
- [3] S. Ji, Y. Chen, X. Wang, Z. Zhang, D. Wang, Y. Li, *Chem. Rev.* **2020**, 120, 11900.
- [4] Z. Li, D. Wang, Y. Wu, Y. Li, *Natl. Sci. Rev.* **2018**, 5, 673.
- [5] Y. Hu, H. Li, Z. Li, B. Li, S. Wang, Y. Yao, C. Yu, *Green Chem.* **2021**, 23, 8754.
- [6] X. Hai, S. Xi, S. Mitchell, K. Harrath, H. Xu, D. F. Akl, D. Kong, J. Li, Z. Li, T. Sun, H. Yang, Y. Cui, C. Su, X. Zhao, J. Li, J. Pérez-Ramírez, J. Lu, *Nat. Nanotechnol.* **2022**, 17, 174.
- [7] Z. Li, B. Li, Y. Hu, X. Liao, H. Yu, C. Yu, *Small Struct.* **2022**, 3, 2200041.
- [8] J. Yang, W. Li, D. Wang, Y. Li, *Small Struct.* **2021**, 2, 2000051.
- [9] A. Suea-Ngam, P. D. Howes, M. Srisa-Art, A. J. deMello, *Chem. Commun.* **2019**, 55, 9895.
- [10] Y. Ding, P. D. Howes, A. J. deMello, *Anal. Chem.* **2020**, 92, 132.
- [11] L. Gutierrez, L. Gomez, S. Irusta, M. Arruebo, J. Santamaria, *Chem. Eng. J.* **2011**, 171, 674.
- [12] S. Marre, K. F. Jensen, *Chem. Soc. Rev.* **2010**, 39, 1183.
- [13] P. Massé, S. Mornet, E. Duguet, M. Tréguer-Delapierre, S. Ravaine, A. Iazzolino, J. B. Salmon, J. Leng, *Langmuir* **2013**, 29, 1790.
- [14] B. Wang, P. Prinsen, H. Wang, Z. Bai, H. Wang, R. Luque, J. Xuan, *Chem. Soc. Rev.* **2017**, 46, 855.
- [15] S. Cho, D.-K. Kang, S. Sim, F. Geier, J.-Y. Kim, X. Niu, J. B. Edel, S.-I. Chang, R. C. R. Wootton, K. S. Elvira, A. J. deMello, *Anal. Chem.* **2013**, 85, 8866.
- [16] A. C. Sun, D. J. Steyer, A. R. Allen, E. M. Payne, R. T. Kennedy, C. R. J. Stephenson, *Nat. Commun.* **2020**, 11, 6202.
- [17] B. J. Hindson, K. D. Ness, D. A. Masquelier, P. Belgrader, N. J. Heredia, A. J. Makarewicz, I. J. Bright, M. Y. Lucero, A. L. Hiddessen, T. C. Legler, T. K. Kitano, M. R. Hodel, J. F. Petersen, P. W. Wyatt, E. R. Steenblock, P. H. Shah, L. J. Bousse, C. B. Troup, J. C. Mellen, D. K. Wittmann, N. G. Erndt, T. H. Cauley, R. T. Koehler, A. P. So, S. Dube, K. A. Rose, L. Montesclaros, S. Wang, D. P. Stumbo, S. P. Hodges, et al., *Anal. Chem.* **2011**, 83, 8604.
- [18] H. Tsunoyama, N. Ichikuni, T. Tsukuda, *Langmuir* **2008**, 24, 11327.
- [19] E. Shahbazali, V. Hessel, T. Noël, Q. Wang, *Nanotechnol. Rev.* **2014**, 3, 65.
- [20] M. Solsona, J. C. Vollenbroek, C. B. M. Tregouet, A.-E. Nieuwelink, W. Olthuis, A. van den Berg, B. M. Weckhuysen, M. Odijk, *Lab. Chip* **2019**, 19, 3575.
- [21] Y. Gao, B. Pinho, L. Torrente-Murciano, *Chem. Eng. J.* **2022**, 432, 134112.
- [22] M. R. Bringer, C. J. Gerdt, H. Song, J. D. Tice, R. F. Ismagilov, *Philos. Trans. A Math. Phys. Eng. Sci.* **2004**, 362, 1087.
- [23] Z. Chen, S. Mitchell, E. Vorobyeva, R. K. Leary, R. Hauert, T. Furnival, Q. M. Ramasse, J. M. Thomas, P. A. Midgley, D. Dontsova, M. Antonietti, S. Pogodin, N. López, J. Pérez-Ramírez, *Adv. Funct. Mater.* **2017**, 27, 1605785.
- [24] Z. Chen, E. Vorobyeva, S. Mitchell, E. Fako, M. A. Ortuño, N. López, S. M. Collins, P. A. Midgley, S. Richard, G. Vilé, J. Pérez-Ramírez, *Nat. Nanotechnol.* **2018**, 13, 702.
- [25] J. P. Brunelle, *Pure Appl. Chem.* **1978**, 50, 1211.
- [26] L. Jiao, J. R. Regalbuto, *J. Catal.* **2008**, 260, 329.
- [27] B. Zhu, P. Xia, W. Ho, J. Yu, *Appl. Surf. Sci.* **2015**, 344, 188.
- [28] J. Probst, P. Howes, P. Arosio, S. Stavrakis, A. deMello, *Anal. Chem.* **2021**, 93, 7673.
- [29] J. Probst, C. N. Borca, M. A. Newton, J. van Bokhoven, T. Huthwelker, S. Stavrakis, A. deMello, *ACS Meas. Sci. Au* **2021**, 1, 27.
- [30] R. Gao, Z. Cheng, A. J. deMello, J. Choo, *Lab. Chip* **2016**, 16, 1022.
- [31] A. Fornell, M. Ohlin, F. Garofalo, J. Nilsson, M. Tenje, *Biomicrofluidics* **2017**, 11, 031101.
- [32] K. Park, J. Park, J. H. Jung, G. Destgeer, H. Ahmed, H. J. Sung, *Biomicrofluidics* **2017**, 11, 064112.
- [33] X. Casadevall i Solvas, X. Niu, K. Leeper, S. Cho, S.-I. Chang, J. B. Edel, A. J. deMello, *J. Vis. Exp. JoVE* **2011**, 58, 3437.
- [34] A. R. Abate, T. Hung, P. Mary, J. J. Agresti, D. A. Weitz, *Proc. Natl. Acad. Sci.* **2010**, 107, 19163.
- [35] D. Hess, T. Yang, S. Stavrakis, *Anal. Bioanal. Chem.* **2020**, 412, 3265.
- [36] R. M. Maceiczky, L. Bezing, A. J. deMello, *React. Chem. Eng.* **2016**, 1, 261.
- [37] X.-M. Zhao, Y. Xia, G. M. Whitesides, *J. Mater. Chem.* **1997**, 7, 1069.
- [38] Z. Chen, S. Mitchell, F. Krumeich, R. Hauert, S. Yakunin, M. V. Kovalenko, J. Pérez-Ramírez, *ACS Sustainable Chem. Eng.* **2019**, 7, 5223.
- [39] S. Büchele, Z. Chen, S. Mitchell, R. Hauert, F. Krumeich, J. Pérez-Ramírez, *ChemCatChem* **2019**, 11, 2812.